Available online at www.sciencedirect.com
ScienceDirect
Trans. Nonferrous Met. Soc. China 23(2013) 3293−3299
Transactions of Nonferrous Metals Society of China
www.tnmsc.cn

Influence of solution temperature on corrosion resistance of Zn−Ca phosphate conversion coating on biomedical Mg−Li−Ca alloys

Rong-chang ZENG[1,2], Xin-xin SUN[1], Ying-wei SONG[2], Fen ZHANG[1], Shuo-qi LI[1], Hong-zhi CUI[1], En-hou HAN[2]

1. College of Material Science and Engineering, Shandong University of Science and Technology, Qingdao 266590, China;
2. State Key Laboratory for Corrosion and Protection, Institute of Metals Research, Chinese Academy of Sciences, Shenyang 110016, China

Received 31 July 2013; accepted 14 October 2013

Abstract: The influence of phosphating bath at different temperatures on the formation and corrosion property of calcium-modified zinc phosphate conversion coating (Zn−Ca−P coating) on Mg−Li−Ca alloy was investigated. The morphologies, elemental distribution and chemical structures of the coatings were examined via SEM, EPMA, EDS, XRD and FT-IR. The corrosion resistance was assessed by hydrogen evolution, potentiodynamic polarization and EIS. The results show that the coating is composed of single element Zn and ZnO at below 45 °C; whereas the coatings are predominantly characterized by $Zn_3(PO_4)_2·4H_2O$ and small amount of element zinc and ZnO at above 50 °C. Mg−Li−Ca alloy with Zn−Ca−P coatings prepared at 55 °C has the highest corrosion resistance. However, the hydrogen evolution rates of the coatings obtained at 40−50 °C is accelerated due to the galvanic corrosion between the imperfection of the single element Zn coating and the Mg substrate.
Key words: magnesium alloy; lithium; calcium; phosphate conversion coating; corrosion; biomaterial

1 Introduction

With a growing need for metallic biomaterials, including stainless steels, cobalt−chromium and titanium alloys, the studies have been focused on their corrosion and surface modification. These alloys have elements such as Cr, Ni and V, which are, to some degree, detrimental to human body [1,2]. Although titanium alloys have an excellent performance, the cost is expensive and they cannot be degradable. However, magnesium alloys exhibit an excellent combination of biocompatibility, biodegradability and mechanical properties homologous to natural bones [1−4]. Currently, the investigations are predominantly concentrated on Mg−Al, Mg−Zn, Mg−Mn, Mg−RE, Mg−Ca and Mg−Li alloys due to their biological functions in human body [5−10]. Among them, Mg−Li-based alloys are the lightest metal, and have utilization in aerospace field and promising applications as biomaterials [2]. Previous literatures [11,12] reported that Mg−Li alloys have some disadvantages, particularly poor corrosion resistance in natural environments. The corrosion of Mg−Li alloys is more serious than that of other Mg alloys because Li is very chemically active [13,14]. It is the poor corrosion resistance that limits the extensive utilization of Mg−Li alloys. Mg−Li alloys must be treated by an appropriate surface modification to improve their corrosion resistance. Recently, numerous coatings have been applied to magnesium alloys, for instance, chemical conversion coating [15−17], microarc oxidation or plasma electrolyte oxidation coating [18,19], chemical plating [20] and polymer coating [21,22]. Among them, the chemical conversion coatings on Mg−Li alloys were studied more because of the obvious advantages, especially low cost and ease in operation. In recent decades, conversion coatings such as stannate [23], phytic acid [24], lanthanum-based [25] and rare earth [26] as well as phosphate conversion film [27] on Mg−Li alloys have been investigated.

Foundation item: Project (51241001) supported by the National Natural Science Foundation of China; Project (ZR2011EMM004) supported by the Natural Science Foundation of Shandong Province, China; Project (SKLCP21012KF03) supported by the Open Foundation of State Key Laboratory for Corrosion and Protection, China; Project (TS20110828) supported by Taishan Scholarship Project of Shandong Province, China
Corresponding author: Rong-chang ZENG; Tel: +86-532-80681226; E-mail: rczeng@foxmail.com
DOI: 10.1016/S1003-6326(13)62866-6

Interestingly, in vivo tests demonstrated that LAE442 alloys (4%Li, 4%Al and 2%RE) have excellent corrosion resistance and good biocompatibility in comparison with AZ91D alloy [28−30]. This result implies that Mg−Li alloys are the most promising magnesium-based biomaterials.

In view of biomedical applications, a combination of both the microstructural and bio-functional designs for the alloys and their coatings should be taken into consideration. While calcium, as the essence of element for human body, was added in the Mg−Li alloy and the phosphating solutions, to improve the corrosion resistance of Mg−Li alloys and modify the traditional phosphate conversion processing. Our prior investigation designated that Mg−Li−Ca alloys had a better corrosion performance than Mg−Ca alloys in Hank's solution due to the formation of dense corrosion products [8].

The introduction of Ca^{2+} as an additive into the zinc phosphate conversion solution led to the formation of calcium modified zinc phosphate conversion (Zn−Ca−P) coatings, which not only promoted the formation of the conversion coating but also refined the microstructure of the coating [31,32], and thus improved the corrosion resistance of AZ31 alloy [32].

This work aims to investigate the effect of solution temperature on the microstructure and corrosion resistance of the Zn−Ca−P coatings on the Mg−Li−Ca alloys for the biomedical applications.

2 Experimental

The experimental material used was Mg−1.3Li−0.6Ca alloy with dimensions of 20 mm×20 mm×5 mm. The samples were ground successively with 150#, 400#, 800#, 1000#, 1500# grit SiC paper, and then polished using 1 μm diamond powder. Prior to the preparation, the samples were firstly degreased and activated in alkaline and acidic solutions, and then cleaned in flow distilled water and dried in cold air between each step of the operation. And in the conversion stage, they were processed in the phosphating bath solution. The composition of the phosphating solutions was 20 g/L Na_2HPO_4, 4 g/L $NaNO_2$, 4 g/L $Zn(NO_3)_2$, 1 g/L NaF and 1 g/L $Ca(NO_3)_2$ with pH of 3 [33]. The pH value of the bath solutions was adjusted to approximately 3 with phosphoric acid. The temperatures of the phosphating solutions were controlled at 40, 45, 50, 55 and 60 °C. All the treatment time was 20 min.

The components of the Mg−Li−Ca substrates and the Zn−Ca−P coatings were analyzed by X-ray diffraction (XRD) and Fourier transform infrared spectroscopy (FT-IR). The surface morphology and the microstructure of the conversion coatings were detected by scanning electron microscopy (SEM). The cross-sectional micrographs and energy-dispersive X-ray spectrum (EDS) spectra were inspected by electron probe micro-analyzer (EPMA). Corrosion characterization was investigated by means of electrochemical measurements and hydrogen evolution. The polarization curves were measured with an electrochemical workstation (PARSTAT, 2273) at a scan rate of 1 mV/s. Three-electrode system was applied. The reference electrode was a saturated calomel electrode (SCE); the counter electrode was a platinum electrode. All the hydrogen evolution tests and the electrochemical measurement were conducted in Hank's solution.

3 Results and discussion

3.1 Influence of temperature on morphologies and chemical compositions of coatings

The distinct SEM morphologies of the Zn−Ca−P coatings are shown in Fig. 1. The temperature is an important influencing factor for the crystal nucleation. From an endothermic perspective, the higher the solution temperature, the quicker the formation of nucleus. Once immersed in the phosphating bath at a pH value of 3, the samples were corroded firstly. At 40 °C, the sample surface showed relatively large and round corrosion pits as well as homogeneously small nucleus (Fig. 1(a)). At 45 °C the nucleus grew bigger and coalesced (Fig. 1(b)). But no crystal hopeite ($Zn_3(PO_4)_2·4H_2O$) had been discerned so far. At 50 °C, the crystal hopeite with a flower-like structure (Fig. 1(c)) could be seen. But the distribution of the crystal was heterogeneous; the surface was incompletely covered with the hopeite and cracks. At temperature of 55 °C, the flower-like structure became bigger and cumulated together, leading to a layer of compact coating with fewer numbers of pores and cracks (Fig. 1(d)). However, when the bath solution temperature reached 60 °C, the coating was full of large size of pores and cracks (Fig. 1(e)). It is noteworthy that the hopeite grew in an epitaxial mode due to the existence of the irregular steps on the surfaces.

The cross-sectional micrograph of Zn−Ca−P coating revealed that the compactness of coatings was denser as the temperature increased. The coating thickness was several micrometers. At the temperatures of 40 °C and 45 °C, obvious corrosion pits can be seen, just as shown in Fig. 1. The adhesion between the coating and the substrate was not very good in accordance with non-typical products in the inserts. At temperature of 55 °C, the micrograph showed that the size of the flower-like structure was larger than the others. The coating (shown in Fig. 2) covered on the surface completely. It is noted that the Zn−Ca−P coating deposited in a corrosion pit as indicated by the arrow in Fig. 2. At 60 °C, the flower-like structure was more

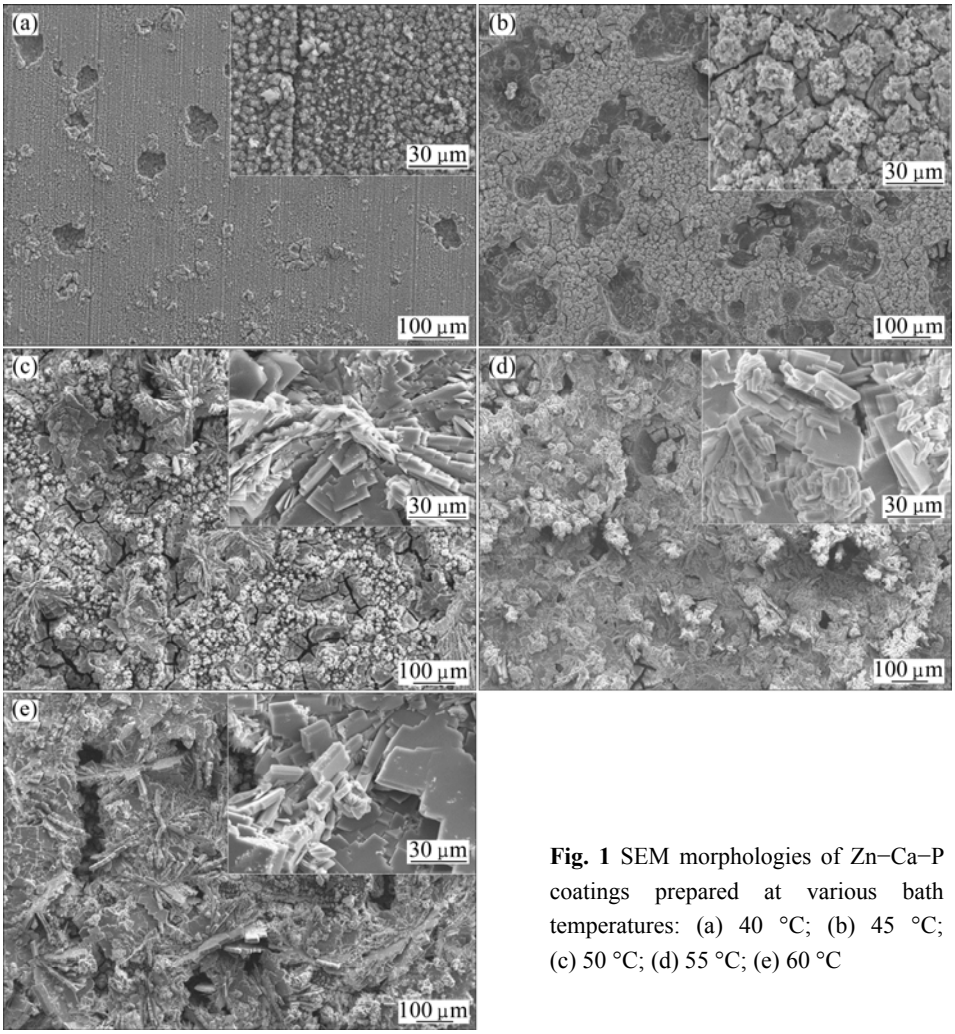

Fig. 1 SEM morphologies of Zn−Ca−P coatings prepared at various bath temperatures: (a) 40 °C; (b) 45 °C; (c) 50 °C; (d) 55 °C; (e) 60 °C

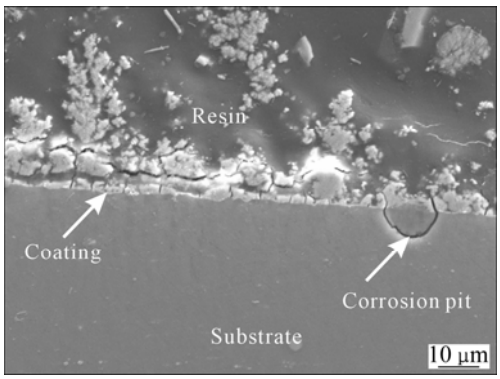

Fig. 2 Cross-sectional micrograph of Zn−Ca−P coating obtained at temperature of 55 °C

homogeneously distributed than the others.

The results of the EDS analysis on the Zn−Ca−P coatings by spot scanning are shown in Table 1. The films are mainly composed of Mg, Zn, Ca, O and P. At a temperature of lower than 50 °C, the amount of Zn element deposited was relatively more, and it arrived at the highest value of 35% at 45 °C. As the temperature increased up to 55 °C, the amount of calcium ascended at the highest, implying the formation of $Ca_3(PO_4)_2$. At 40 °C and 45 °C, zinc was in the form of Zn and ZnO; when the temperature was greater than 50 °C, zinc was predominantly in the form of crystalline $Zn_3(PO_4)_2{\cdot}4H_2O$. The results would be further disclosed by the subsequent XRD pattern in Fig. 3.

Table 1 Average chemical compositions of coatings obtained at various temperatures analyzed by EDS

t/°C	Mass fraction/%				
	Mg	Zn	O	Ca	P
40	6.67	28.34	33.48	3.88	18.92
45	3.26	35.04	25.86	3.33	21.14
50	13.46	23.44	32.74	3.30	17.89
55	8.93	21.35	38.75	7.84	17.77
60	5.48	19.32	33.41	2.84	20.01

3.2 Influence of temperature on phases of phosphate conversion coating

Figure 3 designates that the Zn−Ca−P coating is predominantly composed of $Zn_3(PO_4)_2{\cdot}4H_2O$, little single

substance zinc and a trace of calcium. When the temperature was below 45 °C, zinc formed mainly. When the Mg−Li−Ca alloy was put in the phosphating solutions, magnesium, lithium and calcium were quickly ionized in the corrosion process.

And Zn^{2+} ions in the solution became single substance zinc by obtaining the electrons [34,35]. With increasing temperature, zinc was prone to react with water to generate $Zn(OH)_2$.

$$Zn^{2+}+2e^{-}\longrightarrow Zn \quad (1)$$

$$Zn+2H_2O\longrightarrow Zn(OH)_2+H_2\uparrow \quad (2)$$

$$Zn(OH)_2\longrightarrow ZnO+H_2O \quad (3)$$

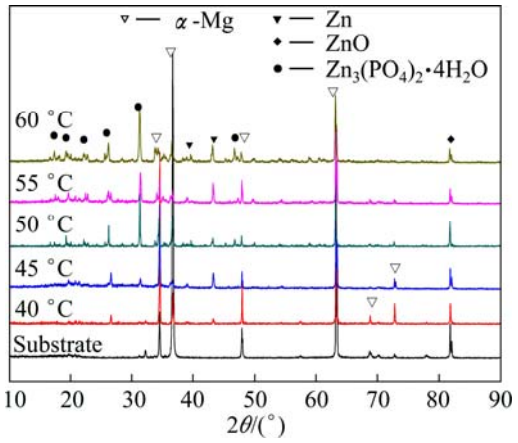

Fig. 3 XRD patterns of coatings obtained at various temperatures

At a pH value of 3, phosphoric acid was decomposed. Magnesium reacting with phosphoric ions led to the formation of hydrogen gas and insoluble magnesium phosphate and zinc phosphate.

$$3Mg+2H^{+}+2H_2PO_4^{-}\rightleftharpoons Mg_3(PO_4)_2+3H_2\uparrow \quad (4)$$

$$3Mg+3Zn^{2+}+4H_2PO_4^{-}+4H_2O\longrightarrow Zn_3(PO_4)_2\cdot 4H_2O+3H_2\uparrow+Mg_3(PO_4)_2+2H^{+} \quad (5)$$

$$ZnO+2H_2PO_4^{-}+2H^{+}\longrightarrow Zn_3(PO_4)_2+3H_2O \quad (6)$$

In fact, $Ca_3(PO_4)_2$ could preferentially deposit in advance of the formation of $Zn_3(PO_4)_2$ [33]. A doped $CaZn_2(PO_4)_2$ was probably produced due to the identical structure between $Ca_3(PO_4)_2$ and $Zn_3(PO_4)_2$ [33, 36].

$$3Ca^{2+}+2PO_4^{3}\longrightarrow Ca_3(PO_4)_2 \quad (7)$$

$$Ca^{2+}+2Zn^{2+}+2H_2PO_4^{-}+2H_2O\longrightarrow CaZn_2(PO_4)\cdot 4H_2O+4H^{+} \quad (8)$$

The FT-IR spectra of Zn−Ca−P coating obtained at various temperatures are shown in Fig. 4. The peaks, appearing at 940−1150 cm^{-1}, are ascribed to the deformation vibration of PO_4^{3-}. The peaks at 3150−3570 cm^{-1} and 1630 cm^{-1} are attributed to OH^{-} because of the water molecules in the coatings. The peaks at 2350 cm^{-1} and 1450 cm^{-1} are assigned to CO_3^{2-} due to the carbon dioxide gas in the air. Although all the infrared absorption peaks correspond to the same location, the intensity of the absorption peaks was different at different temperatures. It is clear that the higher the temperature of the bath solutions, the stronger the intensity of the peaks of PO_4^{3-} and OH^{-}. On the basis of the principle of infrared spectrum, quantitative analysis for the substance can be conducted according to the intensity of absorption. At elevated temperature, the amount of $Zn_3(PO_4)_2\cdot 4H_2O$ and $Ca_3(PO_4)_2$ was more than that at lower temperature.

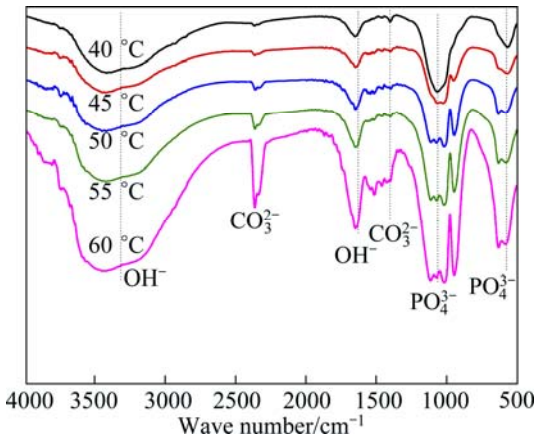

Fig. 4 FT-IR spectra of coatings obtained at various temperatures

Therefore, all the experimental results reveal that the solution temperature exerts a significant influence on the formation of Zn−Ca phosphate conversion coating.

3.3 Influence of temperature on corrosion resistance of conversion coating

Obviously, it is seen from Fig. 5 that the average hydrogen evolution rate at 55 °C was the lowest because the coating was composed of the dense hoplites and $Ca_3(PO_4)_2$. That is, the coating prepared at this temperature

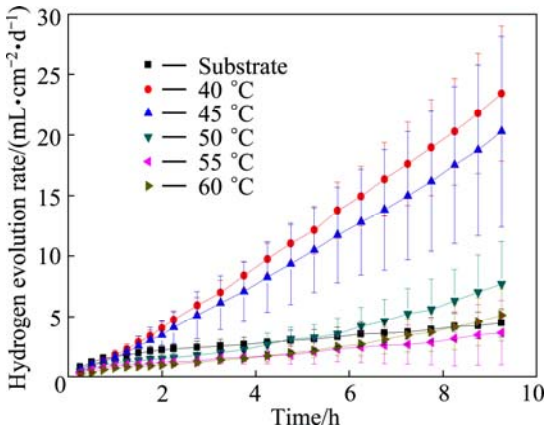

Fig. 5 Hydrogen evolution rate versus time curves of Mg−Li−Ca alloy and its coatings obtained at different temperature

has the best corrosion resistance. The hydrogen evolution rate of the coatings prepared at the bath temperature of 40−50 °C was accelerated due to the galvanic corrosion between the Zn coating and the Mg substrate.

Figure 6 designates the polarization curves of the substrate and the Zn−Ca−P coatings obtained at various temperatures in Hank's solutions. The parameters, derived from the potentiodynamic polarization curves of the coatings, are listed in Table 2. The corrosion current density J_{corr} of the substrate is 19.2 μA/cm^2. It can be seen in Table 2 that the J_{corr} of the coating obtained at 55 °C is the lowest. Thus, the current densities are in good agreement with the hydrogen evolution rates of the corresponding samples.

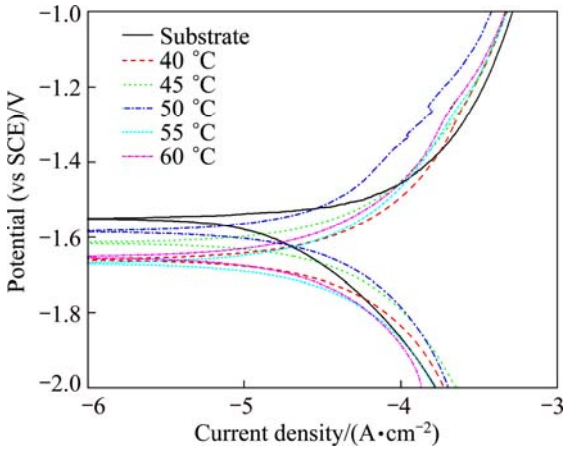

Fig. 6 Polarization curves of substrate and coatings obtained at various temperatures

Table 2 Parameters derived from potentiodynamic polarization curves of Mg−Li−Ca alloy substrate and coatings obtained at various temperatures

t/°C	φ_{corr}(vs SCE)/V	J_{corr}/(μA·cm^{-2})
40	−1.65	23.2
45	−1.62	28.2
50	−1.58	23.4
55	−1.66	17.4
60	−1.65	18.6

This corrosion current density of Mg−Li−Ca alloy with Zn−Ca−P coating obtained at 55 °C is slightly greater than that (11.5 μA/cm^2) of the AZ31 alloy in our earlier work [32]. But the open circuit potential, φ_{corr} (−1.66 V (vs SCE)) of the Mg−Li−Ca alloy with Zn−Ca−P coating is fairly lower than that (−1.50 V (vs SCE)) of the AZ31 alloy with Zn−Ca−P coating [31]. While the φ_{corr} values of the Mg−Li−Ca substrate and AZ31 alloys are −1.55 V (vs SCE) and −1.53 V (vs SCE), respectively. The big difference in φ_{corr} between the two coated alloys remains unclear. It should be pointed out that the corrosion solutions employed are different. The solution for the former is Hank's solution, while for the latter is 3.5% NaCl aqueous solution.

Figure 7 shows the Nyquist plots and Bode plots of the Mg−Li−Ca substrate and its Zn−Ca−P coatings in Hank's solutions. Obviously, the Nyquist diagrams display one high frequency capacitance loop and one low frequency capacitance loop. The low frequency capacitance loop describes the characteristics of the electric double layer. And the high frequency capacitance loop describes the characteristics of the conversion film. The impedance values of various coatings can be obtained from the Bode diagrams. A higher value of

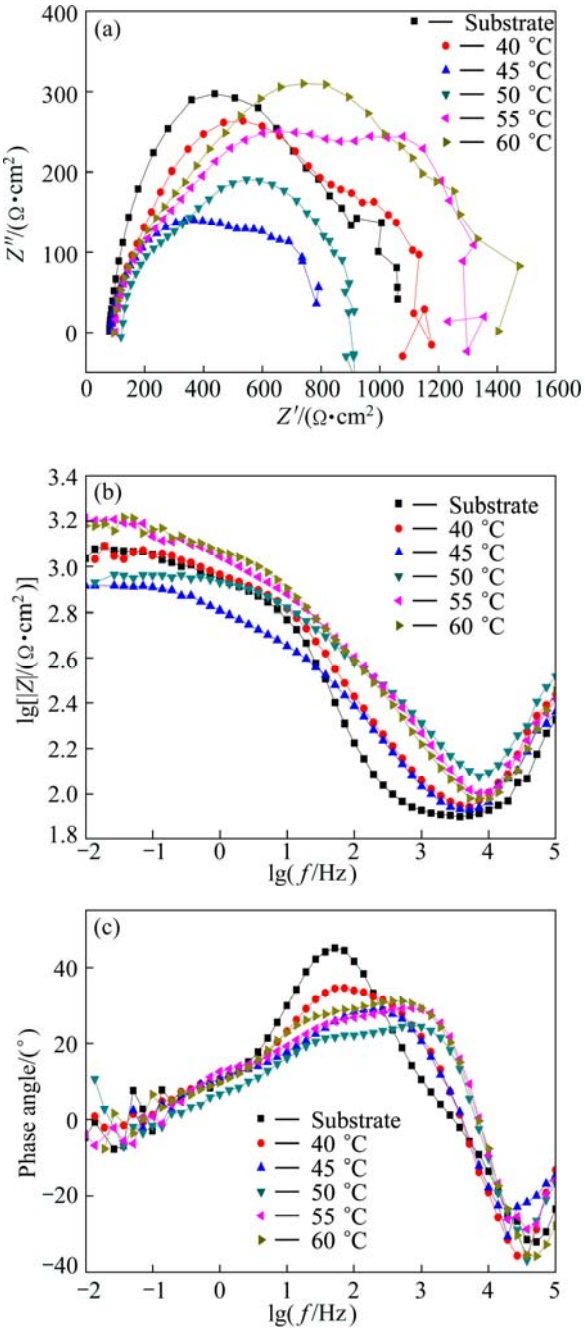

Fig. 7 Nyquist and Bode plots of substrate and coating obtained at various temperatures

impedance means a better corrosion resistance. The results indicate that the corrosion resistance of the coating prepared in the bath at the elevated temperature is better than that obtained at the lower temperatures. To more accurately explain the results in detail, the equivalent circuits of coatings are used to fit the impedance data using ZSimpWin 3.4 software as shown in Fig. 8. The coatings have a much complex equivalent circuit of $R_s(C(R_1(Q(R_2))))$. R_s is the electrolyte resistance. Q is constant phase element (CPE) involving the charge transfer process at the metal/electrolyte interface and related to the dispersion of a capacitance around a mean value [37] and can be modeled by two parameters: Y and n. CPE is used here since it is more suitable to describe the non ideal behavior of the coating, $Z_{CPE}= 1/[Y_0(j\varepsilon)^n]$, with $0\leq n\leq 1$ (for n=1, CPE is an ideal capacitor and therefore Y is equal to a capacitance; for n=0, CPE is a pure resistor and Y=1/R). C and R_1 stand for the characteristics of the conversion film. Q and R_2 stand for the characteristics of the electric double layer. The fitted EIS results of the substrate and coatings obtained at various temperatures are shown in Table 3. At temperature of 55 °C, the value of R_2 is the highest; but the value of R_1 is slightly lower than that at 60 °C. The value of C and Y at 55 °C are lower than that at 60 °C, indicating that the compactness is better than that at 60 °C. However, the improvement in the corrosion resistance of conversion films on Mg−Li−Ca alloy was not obvious.

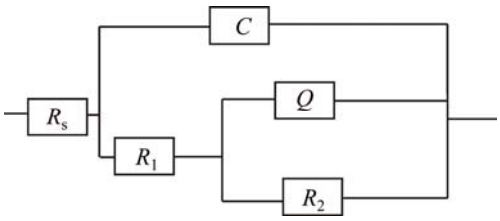

Fig. 8 Fitted equivalent circuit of coatings

Table 3 EIS fitted results for Mg−Li−Ca alloy and coatings obtained at different temperatures

Sample	R_s/ ($\Omega\cdot cm^{-2}$)	C/ ($\mu F\cdot cm^{-2}$)	R_1/ ($\Omega\cdot cm^{-2}$)	Y/ ($\mu\Omega^{-1}\cdot cm^{-2}\cdot s^{-1}$)	n	R_2/ ($\Omega\cdot cm^{-2}$)
Substrate	122	14.7	563	276	0.61	754
40 °C	167	8.02	333	123	0.56	682
45 °C	144	8.03	642	440	0.62	467
50 °C	210	3.07	689	74.5	0.69	310
55 °C	170	2.36	1235	66.6	0.58	945
60 °C	173	2.87	1353	102	0.57	286

4 Conclusions

1) At bath temperatures of 40 °C and 45 °C, the coatings prepared on the Mg−Li−Ca alloys are mainly composed of element Zn and ZnO. While at temperatures higher than 50 °C, the surface is covered with insoluble phosphates: $Zn_3(PO_4)_2\cdot 4H_2O$ and $Ca_3(PO_4)_2$.

2) At 55 °C, the calcium phosphate coupling with $Zn_3(PO_4)_2\cdot 4H_2O$ makes the coatings on the Mg−Li−Ca alloys most dense and compact, which possesses the best corrosion resistance. While the hydrogen evolution rates of the coatings prepared at the bath temperature of 40−50 °C are accelerated due to the galvanic corrosion between the Zn coating and the Mg substrate.

3) The Zn−Ca−P coating on the Mg−Li−Ca alloys only provides a very limited protection. The quality of the coating needs a further improvement.

References

[1] MARK P S, ALEXIS M P, JERAWALA H, GEORGE D. Magnesium and its alloys as orthopedic biomaterials: A review [J]. Biomaterials, 2006, 27(9): 1728−1734.

[2] ZENG R C, DIETZEL W, WITTE F, HORT N, BLAWERT C. Progress and challenge for magnesium alloys as biomaterials [J]. Advanced Engineering Materials, 2008, 10: B03−B14.

[3] SONG Guang-ling, SONG Shi-zhe. A possible biodegradable magnesium implant material [J]. Advanced Engineering Materials, 2007, 9(4): 298−302.

[4] GU Xue-nan, ZHENG Yu-feng, CHENG Yan, ZHONG Sheng-ping, XI Ting-fei. In vitro corrosion and biocompatibility of binary magnesium alloys [J]. Biomaterials, 2009, 30(4): 484−498.

[5] LI Zi-jian, GU Xu-nan, LOU Si-quan, ZHENG Yu-feng. The development of binary Mg–Ca alloys for use as biodegradable materials within bone [J]. Biomaterials, 2008, 29(10): 1329−1344.

[6] GAO Jia-cheng, WU Sha, QIAO Li-ying, WANG Yong. Corrosion behavior of Mg and Mg−Zn alloys in simulated body fluid [J]. Transactions of Nonferrous Metals Society of China, 2008, 18(3): 588−592.

[7] ZHANG Chun-yan, ZENG Rong-chang, LIU Cheng-long, GAO Jia-cheng. Comparison of calcium phosphate coatings on Mg−Al and Mg–Ca alloys and their corrosion behavior in Hank's solution [J]. Surface and Coatings Technology, 2010, 204(21−22): 3636−3640.

[8] ZENG Rong-chang, GUO Xiao-long, LIU Cheng-long, CUI Hong-zhi, TAO Wu. Study on corrosion of medical Mg−Ca and Mg−Li−Ca alloys [J]. Acta Metallurgica Sinica, 2011, 47(11): 1477−1482. (in Chinese)

[9] ZBERG B, UGGOWITZER PETER J, LOEFFLER J F. MgZnCa glasses without clinically observable hydrogen evolution for biodegradable implants [J]. Nature Materials, 2009, 8(11): 887−891.

[10] ZHANG Xiao-bo, YUAN Guang-yin, MAO Lin, NIU Jia-lin, DING Wen-jiang. Biocorrosion properties of as-extruded Mg−Nd−Zn−Zr alloy compared with commercial AZ31 and WE 43 alloys [J]. Materials Letters, 2012, 66(1): 209−211.

[11] ZHANG Chun-hong, HUANG Xiao-mei, ZHANG Mi-lin, GAO Li-li, WU Rui-zhi. Electrochemical characterizarion of the corrosion of a Mg−Li alloy [J]. Materials Letters, 2008, 62(14): 2177−2180.

[12] YANG Guang-yu, HAO Qi-tang, JIE Wan-qi. Study status of Mg−Li system alloys [J]. Foundry Technology, 2004, 25(1): 19−20. (in Chinese)

[13] BRUNELLI K, DABALA M, CALLIARI I, MAGRINI M. Effect of HCl pre-treatment on corrosion resistance of cerium-based conversion coatings on magnesium and magnesium alloys [J]. Corrosion Science, 2005, 47(4): 989−1000.

[14] MOORE K L, SYKES J M, HOGG S C, GRANT P S. Pitting corrosion of spray formed Al−Li−Mg alloys [J]. Corrosion Science, 2008, 50(11): 3221−3226.

[15] van PHUONG N, LEE K, CHANG D, KIM M, LEE S, MOON S. Zinc phosphate conversion coatings on magnesium alloys: A review [J]. Metals and Materials International, 2013, 19(2): 273−281.

[16] JIN He-xi, WANG Ri-chu, PENG Chao-qun, FENG Yan, SHI Kai, CHEN Bin. Research progress of chemical conversion coatings on magnesium alloy [J]. The Chinese Journal of Nonferrous Metals, 2011, 21(9): 2049−2059. (in Chinese)
[17] CHEN Jun, SONG Ying-wei, SHAN Da-yong, HAN En-hou. Properties of dawsonite conversion film on AZ31 magnesium alloy [J]. Transactions of Nonferrous Metals Society of China, 2011, 21(4): 936−942.
[18] SHI P, NG W F, WONG M H, CHENG F T. Improvement of corrosion resistance of pure magnesium in Hanks' solution by micro arc oxidation with sol−gel TiO_2 sealing [J]. Journal of Alloys and Compounds, 2009, 469(1): 286−292.
[19] ZHANG Rong-fa, SHAN Da-yong, HAN En-hou. Status and prospect of anodization on magnesium and its alloys [J]. The Chinese Journal of Nonferrous Metals, 2006, 16(7): 1136−1148. (in Chinese)
[20] SONG Ying-wei, SHAN Da-yong, HAN En-hou. Corrosion behaviors of electroless plating Ni−P coatings deposited on magnesium alloys in artificial sweat solution [J]. Electrochimica Acta, 2007, 53(4): 2009−2015.
[21] ARRABAL R, MOTA J M, CRIADO A, PARDO A, MOHEDANO M, MATYKINA E. Assessment of duplex coating combining plasma electrolytic oxidation and polymer layer on AZ31 magnesium alloy [J]. Surface and Coatings Technology, 2012, 206(22): 4692−4703.
[22] XU L, YAMAMOTO A. Characteristics and cytocompatibility of biodegradable polymer film on magnesium by spin coating [J]. Colloids and Surfaces B: Biointerfaces, 2012, 93: 67−74.
[23] YANG Li-hui, ZHANG Mi-lin, LI Jun-qing, YU Xiang, NIU Zhong-yi. Stannate conversion coatings on Mg−8Li alloy [J]. Journal of Alloys and Compounds, 2009, 471(1): 197−200.
[24] GAO Li-li, ZHANG Chun-hong, ZHANG Mi-lin, HUANG Xiao-mei, XI Jiang. Phytic acid conversion coating on Mg−Li alloy [J]. Journal of Alloys and Compounds, 2009, 485(1): 789−793.
[25] YANG Li-hui, LI Jun-qing, YU Xiang, ZHANG Mi-lin, HUANG Xiao-mei. Lanthanum-based conversion coating on Mg−8Li alloy [J]. Applied Surface Science, 2008, 255(5): 2338−2341.
[26] YANG Xiao-wei, WANG Gui-xiang, DONG Guo-jun, FAN Gong, ZHANG Mi-lin. Rare earth conversion coating on Mg−8.5Li alloys [J]. Journal of Alloys and Compounds, 2009, 487(1): 64−68.
[27] SONG Ying-wei, SHAN Da-yong, CHEN Rong-shi, ZHANG Fan, HAN En-hou. A novel phosphate conversion film on Mg−8.8Li alloy [J]. Surface and Coatings Technology, 2009, 203(9): 1107−1113.
[28] WITTE F, FISCHER J, NELLESEN J, VOGT C, VOGT J, DONATH T, BECKMANN F. In vivo corrosion and corrosion protection of magnesium alloy LAE442 [J]. Acta Biomaterialia, 2010, 6(5): 1792−1799.
[29] WITTE F, FISCHER J, NELLESEN J, CROSTACK H A, KAESE V, PISCH A, WINDHAGEN H. In vitro and in vivo corrosion measurements of magnesium alloys [J]. Biomaterials, 2006, 27(7): 1013−1018.
[30] WITTE F, KAESE V, HAFERKAMP H, SWITZER E, MEYER-LINDENBERG A, WIRTH C J, WINDHAGEN H. In vivo corrosion of four magnesium alloys and the associated bone response [J]. Biomaterials, 2005, 26(17): 3557−3563.
[31] LIU Feng, SHAN Da-yong, HAN En-hou, LIU Chang-sheng. Effect of Ca^{2+} on phosphate conversion coating on magnesium alloy [J]. The Chinese Journal of Nonferrous Metals, 2008, 18(10): 1825−1830. (in Chinese)
[32] ZENG Rong-chang, LAN Zi-dong. Influence of bath temperature of conversion treatment process on corrosion resistance of zinc calcium phosphate conversion film on AZ31 magnesium alloy [J]. The Chinese Journal of Nonferrous Metals, 2010, 20(8): 1461−1466. (in Chinese)
[33] ZENG Rong-chang, LAN Zi-dong, KONG Ling-hong, HUANG Yuan-ding, CUI Hong-zhi. Characterization of calcium-modified zinc phosphate conversion coatings and their influences on corrosion resistance of AZ31 alloy [J]. Surface and Coatings Technology, 2011, 205(11): 3347−3355.
[34] NIU L Y, JIANG Z H, LI G Y, GU C D, LIAN J S. A study and application of zinc phosphate coating on AZ91D magnesium alloy [J]. Surface and Coatings Technology, 2006, 200(9): 3021−3026.
[35] HERSCHKE L, ROTTSTEGGE J, LIEBERWIRTH I, WEGNER G. Zinc phosphate as versatile material for potential biomedical applications [J]. Journal of Materials Science: Materials in Medicine, 2006, 17(1): 81−94.
[36] CHEN X B, BIRBILIS N, ABBOTT T B. Effect of [Ca^{2+}] and [PO_4^{3-}] levels on the formation of calcium phosphate conversion coatings on die-cast magnesium alloy AZ91D [J]. Corrosion Science, 2012, 55: 226−232.
[37] BARCHICHE C E, ROCCA E, JUERS C, HAZAN J, STEINMETZ J. Corrosion resistance of plasma-anodized AZ91D magnesium alloy by electrochemical methods [J]. Electrochimica Acta, 2007, 53(2): 417−425.

溶液温度对医用 Mg−Li−Ca 合金表面锌钙系磷酸盐转化膜耐蚀性能的影响

曾荣昌[1,2]，孙芯芯[1]，宋影伟[2]，张 芬[1]，李硕琦[1]，崔洪芝[1]，韩恩厚[2]

1. 山东科技大学 材料科学与工程学院，青岛 266590；
2. 中国科学院 金属研究所 金属腐蚀与防护国家重点实验，沈阳 110016

摘 要：考察不同磷化液温度对 Mg−Li−Ca 合金表面锌钙磷酸盐转化膜质量和耐蚀性能的影响。利用扫描电子显微镜、电子探针、能谱仪、X 射线衍射和傅里叶红外光谱研究转化膜的表面形貌、化学成分和物相，采用析氢腐蚀实验和动电位电化学技术以及电化学阻抗研究磷化液温度对 Mg−Li−Ca 合金表面磷酸盐转化膜耐蚀性能的影响。结果表明：当溶液温度低于 45 °C 时，膜层主要由 Zn 和 ZnO 组成，而当温度高于 50 °C 时，膜层的主要相为 $Zn_3(PO_4)_2·4H_2O$、少量的 Zn 和 ZnO；在 55 °C 温度下制备的磷酸盐转化膜的耐蚀性能最好；在 40~50 °C 下制备的膜，由于镁基体与锌之间形成的电偶腐蚀而加快了其析氢速率。

关键词：镁合金；锂；钙；磷酸盐转化膜；腐蚀；生物材料

(Edited by Sai-qian YUAN)